

**A heptazine-based polymer photocatalyst with donor-acceptor configuration to promote exciton dissociation and charge separation**

Zhipeng Xie, Wenbin Wang, Xiating Ke, Xu Cai, Xiong Chen,\* Sibowang, Wei Lin, Xincheng Wang\*

State Key Laboratory of Photocatalysis on Energy and Environment, College of Chemistry, Fuzhou University, Fuzhou 350116 P. R. China

Email: chenxiong987@fzu.edu.cn, xcwang@fzu.edu.cn

## **Abstract**

Polymeric carbon nitride (PCN) is an emerging class of polymer semiconductor photocatalysts, but bulk PCN typically suffers from low visible-light-harvesting ability, high activation energy, and rapid charge recombination. In this context, using the same core building block, a donor-acceptor (D-A) type heptazine-based polymer, namely BPCN, was proposed via Friedel-Crafts arylation reaction to tackle these issues. Comparatively, the affording BPCN features extended light absorption, reduced activation energy, and suppressed charge recombination, triggered by the electron push-pull interactions as a consequence of the D-A configuration. BPCN is elucidated to be an effective heterogeneous photocatalyst for aerobic organic transformations and a wide range of substrate scopes and reactions were realized. Besides, BPCN also showed an advantage in mediating the photocatalytic water oxidation reaction, achieving a nearly 10-fold oxygen evolution reaction (OER) rate over PCN. These findings demonstrate the great potential of the rational design of heptazine-based polymers with D-A configurations for artificial photosynthesis.

**Key words:** Polymeric carbon nitride, photocatalysis, organic transformations, oxygen evolution reaction, artificial photosynthesis

## 1. Introduction

Photocatalytic conversion of solar energy has been a hot research topic in the past few decades and numerous attempts have been exerted to developing highly efficient and stable photocatalysts [1-3]. Owing to its environmentally friendly and sustainable features, polymeric carbon nitride (PCN, also known as heptazine-based melon) has been widely regarded as a promising metal-free photocatalyst [4-5]. Since the discover of PCN photocatalyst [4], many post-synthetic modification approaches, including doping [6- 7], copolymerization [8-9], surface interface modification [10], as well as defect engineering [11-12], have been employed to regulate the properties of PCN for high performance photocatalysis.

Building an electron donor-acceptor (D-A) structure is well accepted to effectively improve the exciton dissociation and enable facilitated charge transfer via reducing the charge diffusion length of semiconductors, thereby affording promoted photocatalytic performance [13-18]. The *s*-heptazine moieties, which are typically the main components in PCN scaffold, demonstrated high electron affinity and would be good candidates as acceptors [19-20]. Accordingly, D-A type photocatalysts are envisaged by the incorporation of relatively electron-rich elements/moieties (act as donors) into PCN [21-22]. For instance, Wang et al. have developed a kind of biomimetic D-A photocatalyst (DA-HM), which was delivered by functionalizing heptazine-based melon with selenium and cyanamide [21]. In this manner, the built-in electric field formed in the photocatalyst impels the photoexcited electrons and holes to migrate in opposite directions, resulting in efficient exciton dissociation and restrained charge carriers' recombination, thus boosting the photochemical activity.

However, the traditional thermal condensation of N-rich precursors for PCN fabrication ( $> 500\text{ }^{\circ}\text{C}$ ) makes introducing defined organic fragments into the PCN scaffold in a controlled way difficult and typically results in incomplete polymerization with a relatively limited degree of  $\pi$  electron delocalization in the polymer skeleton, yielding moderate photocatalytic activity. Given this, several mild synthetic strategies have been employed to prepare heptazine-based polymeric photocatalysts with impressive photocatalytic performances, such as nucleophilic substitutions, Schiff base condensations, Friedel-Crafts (F-C) reactions, etc [23-25]. Comparatively, alternative C-C connections could be formed between donor and acceptor motifs with fully  $\pi$ -conjugation via  $\text{AlCl}_3$  catalyzed F-C reactions, which would be beneficial to photocatalysis [25]. Indeed, very recently, several D-A type heptazine-based polymers have been designed via this protocol for efficient photocatalytic hydrogen peroxide production, water splitting, and organic pollutant degradations, etc [19, 20, 25]. Nevertheless, heptazine-based polymer photocatalysis is still insufficiently illustrated, especially in the realm of photocatalytic oxidations.

In this study, a D-A type heptazine-based polymer, namely BPCN, was proposed via F-C reaction for high-performance photocatalytic oxidations. The as-prepared BPCN represents extended light absorption, reduced activation energy, and suppressed charge recombination, triggered by the electron push-pull interactions stemming from the D-A configuration. Accordingly, BPCN demonstrated much higher activity in photocatalytic selective oxidation of sulfides than PCN and a wide range of substrate scopes and reactions were realized under blue LED irradiation. Besides, BPCN also showed an advantage in mediating the photocatalytic water oxidation half-reaction, achieving a nearly 10-fold

oxygen evolution rate (OER) over PCN. This research unravels the potential of the structural design of heptazine-based polymers with D-A architectures for advanced solar-driven photocatalysis.

## **2. Experimental section**

### *2.1 Materials*

Biphenyl was obtained from Shanghai Aladdin Biochemical Technology Co., Ltd. Melamine and sodium hydroxide were provided by Sinopharm Chemical Reagent Co., Ltd. Phosphorus pentachloride was obtained from Adamas Chemical Reagent Co., Ltd. Aluminum chloride was purchased from Alfa Aesar. All chemicals were directly used as received without further purification unless otherwise mentioned.

### *2.2 Polymer preparations*

Polymeric carbon nitride (PCN) [26]: Melamine (10 g) was placed in a porcelain crucible (20 mL), followed by pyrolysis at 550 °C in a furnace for 2 h with a ramp speed of 260 °C/h under air. After being ground by agate mortar, 206 mg of the product was obtained as a powder.

Heptazine polymer (BPCN) [27-29]: Dichloromethane (25 mL), biphenyl (1.8 g, 11.7 mmol), and aluminum trichloride (15.8 mmol 2.11 g) were added into a 50 mL round-bottomed flask, and then slowly adding of cyameluric chloride (2.20 g, 7.8 mmol) in batches. The mixture was stirred at room temperature for 30 minutes first, and then was heated to reflux for 12 h. After cooling, the mixture was poured into ice water with vigorously stirring, filtered, and dried to afford a solid. Further purifying by Soxhlet extraction with ethanol and dichloromethane sequentially to give the target as a purple-yellow powder (yield: 1.1 g).

### 2.3 Characterizations

The Fourier transform infrared (FT-IR) data were recorded on a Nicolet 670 FT-IR spectrometer. The  $^{13}\text{C}$  cross-polarization magic-angle-spinning solid-state NMR ( $^{13}\text{C}$  CP/MAS ssNMR) measurements were conducted on Bruker AVANCE III 500. Elemental analysis (EA) results were collected on Elementar Vario MICRO cube. X-ray photoelectron spectroscopy (XPS) profiles were surveyed on a Thermo ESCALAB250 instrument. X-ray powder diffraction (PXRD) patterns were generated by a Rigaku MiniFlex machine. The  $\text{N}_2$  sorption measurements were performed on Micromeritics 3Flex. Water contact angle measurements were conducted on Dataphysics-OCA20 machine. The scanning emission microscope (SEM) images were observed on Thermo Fisher Verios G4. Transmission electron microscopy (TEM) tests were carried out on FEI TECNAI G2 F20. The energy-dispersive X-ray spectroscopy was examined employing an FEI Super-X energy dispersive spectrum. UV-Vis diffuse reflectance spectra (UV-Vis DRS) were collected on Varian Cary 500 Scan UV-visible system. Photoluminescence (PL) spectra were obtained on an Edinburgh FLS980 spectrophotometer. Photocurrent profiles were collected with a BAS Epsilon Electrochemical System. Gas chromatography-mass (GC-MS) data were generated at Thermo Trace 1300. Analytical GC for the samples was performed on a SHIMADZU GC-2014A TF/SPL machine.

### 2.4 Photocatalytic reactions

Photocatalytic organic transformation: the reaction mixtures were illuminated in a simple photoreactor consisting of Eaglerise ELP8X3LS 3W blue LEDs ( $\lambda = 450 \text{ nm}$ ), which was connected to the HAAKE-FK cyclic water-cooling system. A simple cooling fan was installed above the reactor to control the reaction temperature at  $\sim 25 \text{ }^\circ\text{C}$ , which

was monitored by a standard alcohol thermometer. Reaction conditions: BPCN (10 mg), substrate (0.1 mmol), ethanol (2 mL), air, 450 nm LED (30 W), 25 °C, 1 h, determined by GC-MS.

Photocatalytic water oxidation reaction: photocatalytic O<sub>2</sub> evolution reactions were performed in a Pyrex top-irradiation reaction vessel linked to a glass closed gas circulation system. Typically, 50 mg polymer was thoroughly dispersed in an aqueous solution (100 mL) with the presence of AgNO<sub>3</sub> (0.01 M) as the electron acceptor. Before irradiation under a 300 W Xe lamp and a water-cooling filter, the mixture was evacuated several times to remove air completely. The wavelength of the incident light was controlled by employing an appropriate long pass cut-off filter. The reaction temperature was kept at 12 °C by a flow of cooling water. The generated gases were probed by GC connected with a thermal conductive detector.

Photocatalytic overall water splitting reaction: the operation was the same as photocatalytic O<sub>2</sub> evolution reaction, but without adding any sacrificial agents.

### *2.5 Theoretical calculations*

All the density functional theory (DFT) calculations were conducted using Gaussian 09 software at B3LYP/6-31G (d, p) level of theory [30].

## **3. Results and discussions**

### *3.1 Polymer preparation and characterizations*

BPCN was synthesized by an AlCl<sub>3</sub>-catalyzed F-C arylation reaction between cyameluric chloride and biphenyl under mild condition (**Scheme 1**, details see experimental section and supplementary information). The chemical structure of as-synthesized BPCN was then comprehensively characterized. Both FTIR and <sup>13</sup>C CP/MAS

ssNMR results verified the presence of *s*-heptazine-rings in the skeleton of BPCN (**Fig. 1**). In addition, the signals detected in the range of ~120-150 ppm correspond to the aromatic carbons (**Fig. 1b**). As a control, PCN (heptazine-based melon) was also prepared by pyrolysis of melamine precursor at 550 °C and the chemical structure was verified by both FT-IR and <sup>13</sup>C CP/MAS ssNMR spectra (**Fig. 1**).

### Scheme 1

The surface chemical compositions and element states of BPCN were examined by XPS (**Fig. S1a-b**). The high-resolution C 1s XPS profile of BPCN can be resolved into three peaks centered at ~283.8, 285.6 and 288.0 eV, corresponding to the carbons on the aromatic ring (C-C/C=C), partially hydrolyzed cyameluric chloride (C-O), and the heptazine rings (C-N=C), respectively (**Fig. S1a**). Besides, in the N 1s spectrum, two peaks located at ~398.0 and 399.5 eV stem from the C-N=C and N-(C)<sub>3</sub>, respectively [19, 25], which are similar to PCN sample (**Fig. S1b**). Moreover, the elemental analysis data were close to the theoretical results (**Table S1**), further suggesting the formation of BPCN.

### Fig. 1

The amorphous nature of BPCN was revealed by the PXRD pattern. In contrast, PCN is semicrystalline, in conformity with the reported study (**Fig. S2**) [31]. The porosity of BPCN was verified by nitrogen sorption isotherms conducted at 77 K and the Brunauer-Emmett-Teller (BET) surface area of BPCN was calculated to be 40 m<sup>2</sup>/g, which is obviously higher than PCN (10 m<sup>2</sup>/g, **Fig. S3**). Besides, the contact angle measurements of water on both polymers revealed that the introduction of biphenyl units afforded much enhanced hydrophobicity on the surface of BPCN (71.2 °), in comparison with PCN (30.1 °) (**Fig. S4**). This is likely caused by the decrement in N content for BPCN.



The SEM image of BPCN demonstrated a lamellar structure, similar to PCN (**Fig. S5**). Moreover, the TEM images indicated that BPCN displayed a nanosheet structure with curved surfaces (**Fig. 2a-b**). The high-angle annular dark-field scanning transmission electron microscopy (HAADF STEM) mapping results of BPCN evidenced that C and N were homogeneously distributed inside the polymer (**Fig. 2c-d**).

### **Fig. 2**

#### *3.2 Photophysical and photoelectrochemical properties*

The light-harvesting properties of the polymers were evaluated by UV-vis DRS. Notably, compared with PCN, BPCN exhibits a much stronger light absorption, and the absorption edge could be extended to ~600 nm (**Fig. 3a**), implying the enhanced light-harvesting ability and energy utilization, which could be triggered by the formation of the D-A configuration for BPCN [32]. The bandgaps can be calculated by the Kubelka-Munk function equation to be 2.76 and 2.20 eV for PCN and BPCN (**Fig. S6**), respectively. Besides, the flat-band potential was estimated by the electrochemical Mott-Schottky method (**Fig. S7**) to be -1.17 and -0.64 V for PCN and BPCN, respectively. Accordingly, by combining  $E_g$  with Mott-Schottky plots [33], the band alignments of both polymers can be shown in **Fig. 3b**, clarifying sufficient thermodynamic feasibility to initiate various photocatalytic reactions, e.g., photocatalytic organic transformations, water splitting, etc.

### **Fig. 3**

Temperature-dependent PL profiles of these two polymers were monitored to elucidate the exciton dissociation performances [34-37]. As observed in **Fig. 3c-d**, both polymers experience thermal quenching of their PL emission in the temperature range from 80 to 300 K. Correspondently, by fitting the relevant PL peak intensity in varied

temperatures, the activation energy ( $E_a$ ) can be appraised employing the Arrhenius equation. The  $E_a$  of PCN and BPCN are estimated to be  $\sim 92$  meV and  $\sim 74$  meV, respectively, indicating BPCN is prone to undergo exciton separation more readily, which could be related to the electron push-pull effect in the skeleton for BPCN originating from a D-A structure and may exert a positive effect on the photocatalytic performance. Besides, steady-state PL spectroscopy was used to survey the electron-hole pair recombination efficiency of PCN and BPCN. The fluorescence intensity of BPCN is significantly lower than that of PCN (**Fig. S8**), implying the charge recombination is effectively suppressed in the D-A type polymer, i.e., BPCN [38-39]. This was also clarified by the DFT calculation outcomes (**Fig. S9**), where the HOMO and LUMO orbitals of BPCN were nearly spatially separated, which would greatly reduce the possibility of charge recombination. Further time-resolved fluorescence spectroscopy (TRPL) results showed us the average TRPL lifetime of BPCN ( $\tau = 4.76$  ns) is longer than that of PCN ( $\tau = 3.06$  ns), suggesting a higher charge separation efficiency of BPCN (**Fig. S10**) [40-41].

To further unveil the charge separation behavior in both polymers, photoelectrochemical experiments were carried out. In contrast, BPCN presented a stronger photocurrent response, indicating higher carrier separation efficiency can be generated in BPCN (**Fig. S11**) [42]. Likewise, as revealed by the electrochemical impedance spectroscopy (EIS), BPCN features a significantly smaller semicircle compared with PCN, implying that BPCN demonstrates a decreased charge transfer resistance and more rapid interfacial charge transfer (**Fig. S12**) [43].

### *3.3 Photocatalytic selective oxidation of sulfides*

As a renewable and environmentally friendly method, photocatalytic selective aerobic

oxidation of sulfides represents an important transformation in organic synthesis in the pharmaceutical industry [44-45]. Given this, the photocatalytic performance of BPCN was first demonstrated by selective aerobic oxidation of anisole under blue LED ( $\lambda = 450$  nm, 30 W) irradiation. As depicted in **Fig. 4a**, BPCN demonstrated an over 20 times higher conversion rate than that of PCN under air atmosphere within 1 h. Recycle experiments also showed a conserved high conversion rate and selectivity after 10 cycles (**Fig. 4b**). When BPCN was recovered and re-characterized by PXRD and FTIR, no distinct structural change can be detected before and after the photocatalytic reaction (**Fig. S13**). Such remarkable photocatalytic activity and stability of BPCN may be ascribed to the extended light absorption, reduced  $E_a$ , and suppressed charge recombination, mediated by the electron push-pull interactions as a result of the D-A configuration. Further control experiments verified that air, photocatalyst, and light are the necessary elements for the reaction (**Table S2**). Besides, the conversion rate can be promoted when the reaction was conducted in the pure O<sub>2</sub> atmosphere, suggesting the photocatalytic performance is also related to the O<sub>2</sub> concentration.

#### **Fig. 4**

The wavelength-dependent apparent quantum yield (AQY) of selective oxidation of sulfides over BPCN was also conducted (**Fig. S14**). The tendency of AQY is closely resembled the UV-vis DRS, implying that the photocatalytic conversion is primarily caused by the photo-excited electrons. The AQY of BPCN is determined to be ~8.13% at 420 nm, 5.72% at 450 nm, 2.18% at 500 nm, 1.05% at 520 nm, 0.41% at 600 nm, and 0% at 730 nm, respectively.

The active species of the reaction was determined by trapping experiments, aiming to

speculate on the mechanical process [46]. As shown in **Fig. S15**, the conversion is significantly lowered after adding hydroquinone as a free radical scavenger, implying a free radical process was involved in the photocatalytic oxidation of anisole. Likewise, copper sulfate as an electron scavenger exhibits a significant inhibitory effect. Subsequently, KI, as a hole scavenger, completely inhibits the reaction, revealing the separation of photoinduced electrons and holes. In addition, both *p*-benzoquinone (BQ) ( $\cdot\text{O}_2^-$  scavenger) and TEMPO ( $^1\text{O}_2$  scavenger) can lead to an extremely declined conversion rate. Therefore, photogenerated electrons are responsible for the generation of  $\cdot\text{O}_2^-$  and  $^1\text{O}_2$  active species, which proved to be the key reactive oxygen species (ROS) during the oxidation process.

To further understand the mechanism process and unravel the formation of  $^1\text{O}_2$  and  $\cdot\text{O}_2^-$  during the photocatalytic reaction, EPR tests were performed (**Fig. S16**) [47-48]. EPR signal disappears when DMPO or TEMPO was added as a capture agent without light irradiation. In contrast, the corresponding DMPO- $\cdot\text{O}_2^-$  and TEMPO- $^1\text{O}_2$  adduct signals can be observed upon visible-light illumination. Moreover, the intensity of the EPR signals strengthened with the prolonged exposure time, further demonstrating the generation of  $\cdot\text{O}_2^-$  and  $^1\text{O}_2$  toward light irradiation. On the one hand, regarding the estimated electronic band structure, there were sufficient thermodynamic driving forces for BPCN to enable the occurrence of  $\text{O}_2/\cdot\text{O}_2^-$  transformation ( $E = -0.33$  V vs. NHE, **Fig. 3b**) in the CB and single electron oxidation of thioanisole ( $E = 1.30$  V vs. NHE, **Fig. S17**) in the VB [49], respectively, allowing a smooth electron transfer process. On the other hand, the extended  $\pi$ - $\pi$  conjugated framework of BPCN can facilitate ground-state oxygen ( $^3\text{O}_2$ ) to yield  $^1\text{O}_2$  via triplet energy transfer. Accordingly, both  $\cdot\text{O}_2^-$  and  $^1\text{O}_2$  were generated in BPCN and

participated in the photocatalytic reaction, and a plausible photocatalytic process can be proposed. As portrayed in **Fig. 5**, the photocatalytic selective oxidation of anisole by BPCN may follow two routes (i.e., electron and energy transfer pathways) under 450 nm LED irradiation. In the electron transfer pathway, oxygen is reduced by photoexcited electrons to initiate  $\cdot\text{O}_2^-$ , anisole is oxidized by photoinduced holes to the corresponding cationic free radical intermediates, and then  $\cdot\text{O}_2^-$  reacts with the S radical cation and is converted into the final product. In the case of the energy transfer route,  $\text{O}_2$  is first converted into  $^1\text{O}_2$  through energy transfer between the triplet excited state of BPCN and  $^3\text{O}_2$ , and then benzyl sulfide is oxidized by singlet oxygen to benzyl sulfoxide.

**Fig. 5**

#### *3.4 Scope for the photocatalytic oxidation of sulfides*

Encouraged by the impressive photocatalytic activity stated above, we then extended the substrate scope to some other sulfide derivatives aiming to explore the universality of the photocatalytic performance for BPCN. Using the standard oxidation condition, various thioanisole-based compounds with different substituent groups on the phenyl rings, i.e., electron-withdrawing moieties of  $-\text{NO}_2$ , and  $-\text{Br}$  (entries 1-2 in **Table 1**) and electron-donating motifs of  $-\text{Me}$  and  $-\text{OMe}$  (entries 4-5 in **Table 1**), were first examined. As listed in **Table 1**, sulfides with electron-donating groups generally exhibited a higher conversion rate, while a much lower conversion rate, even nearly completely inhibited, was demonstrated when electron-withdrawing groups were anchored, which was also observed in a previous study [50]. Besides, the influence of steric hindrance on their conversion rate was studied (entries 6-7 in **Table 1**), where an enhanced steric hindrance of the substrate led to a gradual decrease in the conversion rate [51].

### Table 1

Furthermore, the potential application of BPCN for the selective transformation of other organic molecules, including the dehydrogenation of aminobenzene, and the hydroxylation of phenylboronic acid was tested. As shown in **Table 2**, nearly quantitative conversion and selectivity were realized in these two types of reactions. The above-mentioned photocatalytic profile is green and mild, endowing BPCN with great application potential in solar-driven aerobic organic transformations.

### Table 2

#### *3.5 Photocatalytic oxygen evolution and hydrogen generation reactions*

Conjugated polymers have been recognized as promising supplements to inorganic photocatalysts for photocatalytic water splitting. Fundamentally, photocatalytic overall water splitting process involves two half-catalytic reactions, i.e., the hydrogen evolution reaction (HER) and the oxygen evolution reaction (OER). The total reaction rate is mainly relied on the OER, because the OER is a four-electron process with slow kinetics and multi-electron transfer, consisting of the cleavage of O-H bonds and the generation of O-O bonds [52-54].

### Fig. 6

Herein, in viewing the appropriate VB level, it is highly possible that photocatalytic OER could be initiated in the presence of BPCN. Accordingly, the photocatalytic behavior of the as-synthesized BPCN was further investigated by OER containing silver nitrate ( $\text{AgNO}_3$ ) as the electron scavenger under visible-light illumination. Indeed, as displayed in **Fig. 6a**, BPCN can mediate the OER even without the aid of a cocatalyst, reaching  $\sim 15.2 \mu\text{mol h}^{-1}$  for 50 mg polymer sample. When 3% Co was *in-situ* loaded, the photocatalytic

OER rate could be further boosted to  $\sim 33 \mu\text{mol h}^{-1}$  for BPCN, over 10-fold that of the PCN sample. Besides, a long-term OER test was carried out with both materials to elucidate the stability of the photocatalyst. As can be seen in **Fig. 6b**, the total amount of evolved  $\text{O}_2$  reached  $\sim 8.3$  and  $\sim 68.8 \mu\text{mol}$  for PCN and BPCN after 6 h visible-light irradiation, respectively. When the reaction times were prolonged, the OER rate decreased gradually. This may be stemmed from the light shading effect caused by the formation of Ag nanoparticles on the surface of the photocatalyst (afforded by the photoreduction of  $\text{Ag}^+$ ), resulting in a hindered optical absorption [55]. Besides, BPCN also demonstrated a much higher average HER rate ( $\sim 13.0 \mu\text{mol h}^{-1}$ ) than that of the PCN ( $\sim 1.0 \mu\text{mol h}^{-1}$ ) upon visible-light irradiation (**Fig. 6c**). The much higher photocatalytic activities of the BPCN over PCN in both half-reactions further emphasize the advantage of constructing D-A configuration on photocatalytic performance. We further performed photocatalytic overall water splitting experiment employing BPCN as the photocatalyst with 1% Co and 3% Pt as the co-catalysts. However, there are no  $\text{H}_2$  and  $\text{O}_2$  could be detected even under UV light irradiation. In fact, the realization of photocatalytic overall water splitting by polymeric photocatalysts is challenging, since the behavior of overall water splitting is a complex interplay of the photon absorption, charge carrier dissociation and transport at the band positions, the wettability of their surfaces, and metal co-catalysts, etc [56-57]. Here, although BPCN possesses suitable band structures for photocatalytic overall water splitting, the much lower photocatalytic activity in the  $\text{H}_2$  generation half-reaction likely exerts an influence on the overall reaction, since the kinetics of both half reactions are difficult to balance to facilitate overall water splitting [57].

#### **4. Conclusion**

In summary, a heptazine-based D-A type polymer, namely BPCN, has been proposed via the simple F-C alkylation reaction. The affording BPCN features narrowed optical bandgap, spatially separated HOMO and LUMO delocalization and lowered activation energy, leading to extended light absorption capability, promoted exciton dissociation, boosted charge transfer, and suppressed charge recombination. These features would presumably be beneficial to the photocatalysis. Indeed, BPCN is highly active in photocatalytic aerobic organic transformations and a wide range of substrate scopes and reactions were realized. Besides, BPCN also showed an advantage in mediating the photocatalytic water oxidation half-reaction, achieving a nearly 10-fold OER rate over PCN. This study demonstrates the great potential of rational design of heptazine-based polymers with D-A configurations toward high-performance solar-driven artificial photosynthesis.

### **Declaration of Competing Interest**

The authors declare that they have no competing financial interest.

### **Acknowledgment**

This work was financially supported by the National Key R&D Program of China (2021YFA1502100), the National Natural Science Foundation of China (21972021, U1905214 and 22111530111), the National Basic Research Program of China (2013CB632405), the Chang Jiang Scholars Program of China (T2016147), and the 111 Project (D16008).

### **REFERENCES**

[1] J. Zhang, X. Chen, K. Takanebe, K. Maeda, K. Domen, J. D. Epping, X. Fu, M. Antonietti, X. Wang,



Synthesis of a Carbon Nitride Structure for Visible-Light Catalysis by Copolymerization, *Angew. Chem. Int. Ed.* 49 (2010) 441-444.

[2] Y. Du, H. Sheng, D. Astruc, M. Zhu, Atomically Precise Noble Metal Nanoclusters as Efficient Catalysts: A Bridge between Structure and Properties, *Chem. Rev.* 120 (2020) 526-622.

[3] C. Wu, N. Corrigan, C. H. Lim, W. Liu, G. Miyake, C. Boyer, Rational Design of Photocatalysts for Controlled Polymerization: Effect of Structures on Photocatalytic Activities, *Chem. Rev.* 122 (2022) 5476-5518.

[4] X. Wang, K. Maeda, A. Thomas, K. Takanebe, G. Xin, J. M. Carlsson, K. Domen, M. Antonietti, A metal-free polymeric photocatalyst for hydrogen production from water under visible light, *Nat. Mater.* 8 (2009) 76-80.

[5] L. Yang, Y. Peng, X. Luo, Y. Dan, J. Ye, Y. Zhou, Z. Zou, Beyond  $C_3N_4$   $\pi$ -conjugated metal-free polymeric semiconductors for photocatalytic chemical transformations, *Chem. Soc. Rev.* 50 (2021) 2147-2172.

[6] W. Lei, Y. Mi, R. Feng, P. Liu, S. Hu, J. Yu, X. Liu, J. A. Rodriguez, J. O. Wang, L. Zheng, K. Tang, S. Zhu, G. Liu, M. Liu, Hybrid 0D-2D black phosphorus quantum dots-graphitic carbon nitride nanosheets for efficient hydrogen evolution, *Nano Energy* 50 (2018) 552-561.

[7] Y. Huang, D. Li, Z. Fang, R. Chen, B. Luo, W. Shi, Controlling carbon self-doping site of g- $C_3N_4$  for highly enhanced visiblelight-driven hydrogen evolution, *Appl. Catal. B: Environ.* 254 (2019) 128-134.

[8] J. Zhang, G. Zhang, X. Chen, S. Lin, L. Mohlmann, G. Dolega, G. Lipner, M. Antonietti, S. Blechert, X. Wang, Co-Monomer Control of Carbon Nitride Semiconductors to Optimize Hydrogen Evolution with Visible Light, *Angew. Chem. Int. Ed.* 51 (2012) 3183-3187.

[9] M. Han, C. Kang, Z. Qu, S. Zhu, B. Yang, Surface molecule induced effective light absorption and charge transfer for  $H_2$  production photocatalysis in a carbonized polymer dots-carbon nitride system, *Appl. Catal. B: Environ.* 305 (2022) 121064.

[10] Z. Zhou, Y. Zhang, Y. Shen, S. Liu, Y. Zhang, Molecular engineering of polymeric carbon nitride: advancing applications from photocatalysis to biosensing and more, *Chem. Soc. Rev.* 47 (2018) 2298-2321.

[11] P. Yang, H. Zhuzhang, R. Wang, W. Lin, X. Wang, Carbon Vacancies in a Melon Polymeric Matrix Promote Photocatalytic Carbon Dioxide Conversion, *Angew. Chem. Int. Ed.* 58 (2019) 1134-1137.

[12] X. Zhang, P. Ma, C. Wang, L. Gan, X. Chen, P. Zhang, Y. Wang, H. Li, L. Wang, X. Zhou, K. Zheng,

Unraveling the dual defect sites in graphite carbon nitride for ultra-high photocatalytic H<sub>2</sub>O<sub>2</sub> evolution, *Energy Environ. Sci.* 15 (2022) 830-842.

[13] Z. A. Lan, W. Ren, X. Chen, Y. Zhang, X. Wang, Conjugated donor-acceptor polymer photocatalysts with electron-output “tentacles” for efficient hydrogen evolution, *Appl. Catal. B: Environ.* 245 (2019) 596-603.

[14] Y. Zhong, M. Causa, G. J. Moore, P. Krauspe, B. Xiao, F. Gunther, J. Kublitski, R. Shivhare, J. Benduhn, E. BarOr, S. Mukherjee, K. M. Yallum, J. Rehault, S. C. B. Mannsfeld, D. Neher, L. J. Richter, D. M. DeLongchamp, F. Ortmann, K. Vandewal, E. Zhou, N. Banerji, Sub-picosecond charge-transfer at near-zero driving force in polymer:non-fullerene acceptor blends and bilayers, *Nat. Commun.* 11 (2020) 833.

[15] Y. Jiao, L. Dordevic, H. Mao, R. M. Young, T. Jaynes, H. Chen, Y. Qiu, K. Cai, L. Zhang, X. Y. Chen, Y. Feng, M. R. Wasielewski, S. I. Stupp, J. F. Stoddart, A Donor-Acceptor [2] Catenane for Visible Light Photocatalysis, *J. Am. Chem. Soc.* 143 (2021) 8000-8010.

[16] C. Han, S. Xiang, P. Xie, P. Dong, C. Shu, C. Zhang, J. X. Jiang, A Universal Strategy for Boosting Hydrogen Evolution Activity of Polymer Photocatalysts under Visible Light by Inserting a Narrow-Band-Gap Spacer between Donor and Acceptor, *Adv. Funct. Mater.* 32 (2022) 2109423.

[17] Z. Li, H. Fang, Z. Chen, W. Zou, C. Zhao, X. Yang, Regulating donor-acceptor interactions in triazine-based conjugated polymers for boosted photocatalytic hydrogen production, *Appl. Catal. B: Environ.* 312 (2022) 121374

[18] C. Han, S. Xiang, M. Ge, P. Xie, C. Zhang, J. X. Jiang, An Efficient Electron Donor for Conjugated Microporous Polymer Photocatalysts with High Photocatalytic Hydrogen Evolution Activity, *Small* 18 (2022) 2202072.

[19] H. Cheng, H. Lv, J. Cheng, L. Wang, X. Wu, H. Xu, Rational Design of Covalent Heptazine Frameworks with Spatially Separated Redox Centers for High-Efficiency Photocatalytic Hydrogen Peroxide Production, *Adv. Mater.* 34 (2022) 2107480.

[20] Y. Zhao, C. Wang, X. Han, Z. Lang, C. Zhao, L. Yin, H. Sun, L. Yan, H. Ren, H. Tan, Two-Dimensional Covalent Heptazine-Based Framework Enables Highly Photocatalytic Performance for Overall Water Splitting, *Adv Sci.* 9 (2022) 2202417.

[21] H. Ou, X. Chen, L. Lin, Y. Fang, X. Wang, Biomimetic Donor-Acceptor Motifs in Conjugated Polymers

for Promoting Exciton Splitting and Charge Separation, *Angew. Chem. Int. Ed.* 57 (2018) 8729-8733.

[22] H. Wang, H. Cheng, H. Lv, H. Xu, X. Wu, J. Yang, Molecular Design of Two-Dimensional Covalent Heptazine Frameworks for Photocatalytic Overall Water Splitting under Visible Light, *J. Phys. Chem. Lett.* 13 (2022) 3949-3956.

[23] K. Kailasam, J. Schmidt, H. Bildirir, G. Zhang, S. Blechert, X. Wang, A. Thomas, Room Temperature Synthesis of Heptazine-Based Microporous Polymer Networks as Photocatalysts for Hydrogen Evolution, *Macromol. Rapid Commun.* 34 (2013) 1008-1013.

[24] W. Zhang, C. Xu, T. Kobayashi, Y. Zhong, Z. Guo, H. Zhan, M. Pruski, W. Huang, Hydrazone-Linked Heptazine Polymeric Carbon Nitrides for Synergistic Visible-Light-Driven Catalysis, *Chem. Eur J.* 26 (2020) 7358-7364.

[25] Z. Li, W. Zeng, M. H. Li, J. F. Zheng, X. Fang, M. J. Lin, Donor-Acceptor Conjugated Heptazine Polymers with Highly Efficient Photocatalytic Degradations towards Tetracyclines, *Macromol. Rapid Commun.* 42 (2021) 2100577.

[26] G. Li, Z. Xie, S. Chai, X. Chen, X. Wang, A facile one-step fabrication of holey carbon nitride nanosheets for visible-light-driven hydrogen evolution, *Appl. Catal. B: Environ.* 283 (2021) 119637.

[27] J. Li, T. Nakagawa, J. MacDonald, Q. Zhang, H. Nomura, H. Miyazaki, C. Adachi, Highly Efficient Organic Light-Emitting Diode Based on a Hidden Thermally Activated Delayed Fluorescence Channel in a Heptazine Derivative, *Adv. Mater.* 25 (2013) 3319.

[28] E. J. Rabe, K. L. Corp, A. L. Sobolewski, W. Domcke, C. W. Schlenke, Proton-Coupled Electron Transfer from Water to a Model Heptazine-Based Molecular Photocatalyst, *J. Phys. Chem. Lett.* 9 (2018) 6257.

[29] J. F. Zheng, Z. P. Xie, Z. Li, Y. Chen, X. Fang, X. Chen, M. J. Lin, Structural design of small-molecule carbon-nitride dyes for photocatalytic hydrogen evolution, *Dyes Pigm.* 185 (2021) 108946.

[30] Gaussian 09, Revision A.02, M. J. Frisch, G. W. Trucks, H. B. Schlegel, G. E. Scuseria, M. A. Robb, J. R. Cheeseman, G. Scalmani, V. Barone, G. A. Petersson, H. Nakatsuji, X. Li, M. Caricato, A. Marenich, J. Bloino, B. G. Janesko, R. Gomperts, B. Mennucci, H. P. Hratchian, J. V. Ortiz, A. F. Izmaylov, J. L. Sonnenberg, D. Williams-Young, F. Ding, F. Lipparini, F. Egidi, J. Goings, B. Peng, A. Petrone, T. Henderson, D. Ranasinghe, V. G. Zakrzewski, J. Gao, N. Rega, G. Zheng, W. Liang, M. Hada, M. Ehara, K. Toyota, R.

Fukuda, J. Hasegawa, M. Ishida, T. Nakajima, Y. Honda, O. Kitao, H. Nakai, T. Vreven, K. Throssell, J. A. Montgomery, Jr., J. E. Peralta, F. Ogliaro, M. Bearpark, J. J. Heyd, E. Brothers, K. N. Kudin, V. N. Staroverov, T. Keith, R. Kobayashi, J. Normand, K. Raghavachari, A. Rendell, J. C. Burant, S. S. Iyengar, J. Tomasi, M. Cossi, J. M. Millam, M. Klene, C. Adamo, R. Cammi, J. W. Ochterski, R. L. Martin, K. Morokuma, O. Farkas, J. B. Foresman, D. J. Fox, Gaussian, Inc., Wallingford CT, 2016.

[31] G. Zhang, C. Huang, X. Wang, Dispersing Molecular Cobalt in Graphitic Carbon Nitride Frameworks for Photocatalytic Water Oxidation, *Small* 11 (2015) 1215-1221.

[32] C. Xu, X. Liu, H. Liu, D. Li, Y. Yang, S. Lin, D. Fan, H. Pan, Molecular engineering for constructing a D-A system and enhancing delocalization in g-C<sub>3</sub>N<sub>4</sub> with superior photocatalytic activity, *J. Mater. Chem. A* 10 (2022) 21031-21043.

[33] C. Wang, Q. Wan, J. Cheng, S. Lin, A. Savateev, M. Antonietti, X. Wang, Efficient aerobic oxidation of alcohols to esters by acidified carbon nitride photocatalysts, *J. Catal.* 393 (2021) 116-125.

[34] Z. A. Lan, G. Zhang, X. Chen, Y. Zhang, K. A. I. Zhang, X. Wang, Reducing the Exciton Binding Energy of Donor-Acceptor-Based Conjugated Polymers to Promote Charge-Induced Reactions, *Angew. Chem. Int. Ed.* 58 (2019) 10236-10240.

[35] Z. A. Lan, M. Wu, Z. Fang, X. Chi, X. Chen, Y. Zhang, X. Wang, A Fully Coplanar Donor-Acceptor Polymeric Semiconductor with Promoted Charge Separation Kinetics for Photochemistry, *Angew. Chem. Int. Ed.* 60 (2021) 16355-16359.

[36] S. Chai, X. Chen, X. Zhang, Y. Fang, R. S. Sprick, X. Chen, Rational design of covalent organic frameworks for efficient photocatalytic hydrogen peroxide production, *Environ. Sci. Nano* 9 (2022) 2464-2469.

[37] W. Wang, H. Wang, X. Tang, J. Huo, Y. Su, C. Lu, Y. Zhang, H. Xu, C. Gu, Phenothiazine-based covalent organic frameworks with low exciton binding energies for photocatalysis, *Chem. Sci.* 13 (2022) 8679-8685.

[38] Z. A. Lan, Y. Fang, X. Chen, X. Wang, Thermal annealing-induced structural reorganization in polymeric photocatalysts for enhanced hydrogen evolution, *Chem. Commun.* 55 (2019) 7756-7759.

[39] F. Zhang, J. Ma, Y. Tan, G. Yu, H. Qin, L. Zheng, H. Liu, R. Li, Construction of Porphyrin Porous Organic Cage as a Support for Single Cobalt Atoms for Photocatalytic Oxidation in Visible Light, *ACS Catal.* 12 (2022) 5827-5833.

- [40] P. Cai, M. Xu, S. S. Meng, Z. Lin, T. Yan, H. F. Drake, P. Zhang, J. Pang, Z. Y. Gu, H. C. Zhou, Precise Spatial-Designed Metal-Organic-Framework Nanosheets for Efficient Energy Transfer and Photocatalysis, *Angew. Chem. Int. Ed.* 60 (2021) 27258-27263.
- [41] Y. Guo, Q. Zhou, J. Nan, W. Shi, F. Cui, Y. Zhu, Perylenetetracarboxylic acid nanosheets with internal electric fields and anisotropic charge migration for photocatalytic hydrogen evolution, *Nat. Commun.* 13 (2022) 2067.
- [42] Y. Yang, N. Luo, S. Lin, H. Yao, Y. Cai, Cyano Substituent on the Olefin Linkage: Promoting Rather than Inhibiting the Performance of Covalent Organic Frameworks, *ACS Catal.* 12 (2022) 10718-10726.
- [43] G. Li, Z. Xie, Q. Wang, X. Chen, Y. Zhang, X. Wang, Asymmetric Acceptor-Donor-Acceptor Polymers with Fast Charge Carrier Transfer for Solar Hydrogen Production. *Chem. Eur. J.* 27 (2021) 939-943.
- [44] Q. Li, X. Lan, G. An, L. Ricardez-Sandoval, Z. Wang, G. Bai, Visible-Light-Responsive Anthraquinone Functionalized Covalent Organic Frameworks for Metal-Free Selective Oxidation of Sulfides: Effects of Morphology and Structure, *ACS Catal.* 10 (2020) 6664-6675.
- [45] X. Ma, H. Hao, W. Sheng, F. Huang, X. Lang, Bridging green light photocatalysis over hierarchical Nb<sub>2</sub>O<sub>5</sub> for the selective aerobic oxidation of sulfides, *J. Mater. Chem. A.* 9 (2021) 2214-2222.
- [46] J. Wang, X. Xu, Y. Liu, Z. Wang, P. Wang, Z. Zheng, H. Cheng, Y. Dai, B. Huang, Oxygen-Vacancy-Enhanced Singlet Oxygen Production for Selective Photocatalytic Oxidation, *ChemSusChem* 13 (2020) 3488-3494.
- [47] F. Zhang, H. Hao, X. Dong, X. Li, X. Lang, Olefin-linked covalent organic framework nanotubes based on triazine for selective oxidation of sulfides with O<sub>2</sub> powered by blue light, *Appl. Catal. B: Environ.* 305 (2022) 121027.
- [48] F. Zhang, X. Ma, X. Dong, X. Miao, X. Lang, Inserting acetylene into an olefin-linked covalent organic framework for boosting the selective photocatalytic aerobic oxidation of sulfides, *Chem. Eng. J.* 451 (2023) 138802.
- [49] Conjugated porous polymer based on BOPHY dyes as photocatalyst under visible light, C. G. López-Calixto, S. Cabrerab, R. Pérez-Ruiz, M. Barawi, J. Alemán, V. A. de la Peña O'Shea, M. Lirasa, *Appl. Catal. B: Environ.* 258 (2019) 117933.
- [50] X. Ma, X. Lang, Titanate nanotube confined merger of organic photocatalysis and TEMPO catalysis for

highly selective aerobic oxidation of sulfides, *Sustain. Energy & Fuels*. 4 (2020) 1754-1763.

[51] J. L. Shi, X. Lang, Assembling polydopamine on TiO<sub>2</sub> for visible light photocatalytic selective oxidation of sulfides with aerial O<sub>2</sub>, *Chem. Eng. J.* 392 (2020) 123632.

[52] Y. Duan, B. Chakraborty, C. K. Tiwari, M. Baranov, T. Tubul, N. Leffler, A. Neyman, I. A. Weinstock, Solution-State Catalysis of Visible Light-Driven Water Oxidation by Macroanion-Like Inorganic Complexes of  $\gamma$ -FeOOH Nanocrystals, *ACS Catal.* 11 (2021) 11385-11395.

[53] Y. Fang, Y. Hou, X. Fu, X. Wang, Semiconducting Polymers for Oxygen Evolution Reaction under Light Illumination, *Chem. Rev.* 122 (2022) 4204-4256.

[54] M. L. Xu, M. Lu, G. Y. Qin, X. M. Wu, T. Yu, L. N. Zhang, K. Li, X. Cheng, Y. Q. Lan, Piezo-Photocatalytic Synergy in BiFeO<sub>3</sub>@COF Z-Scheme Heterostructures for High-Efficiency Overall Water Splitting, *Angew. Chem. Int. Ed.* 61 (2022) e202210700.

[55] Z. Zhong, J. Liu, X. Xu, A. Cao, Z. Tao, W. You, L. Kang, Synthesis of Z-scheme cobalt porphyrin/nitrogen-doped graphene quantum dot heterojunctions for efficient molecule-based photocatalytic oxygen evolution, *J. Mater. Chem. A*. 9 (2021) 404-2413.

[56] M. Rahman, H. Tian, T. Edvinsson, Revisiting the Limiting Factors for Overall Water-Splitting on Organic Photocatalysts, *Angew. Chem. Int. Ed.* 59 (2020) 16278.

[57] Y. Bai, C. Li, L. Liu, Y. Yamaguchi, M. Bahri, H. Yang, A. Gardner, M. A. Zwiijnenburg, N. D. Browning, A. J. Cowan, A. Kudo, A. I. Cooper, R. S. Sprick, Photocatalytic Overall Water Splitting Under Visible Light Enabled by a Particulate Conjugated Polymer Loaded with Palladium and Iridium, *Angew. Chem. Int. Ed.* 61 (2022) e202201299.

## Captions for Schemes, Figures and Tables

**Scheme 1.** Schematic representation of the synthesis of (a) PCN (heptazine-based melon) and (b) BPCN. (c) DFT geometry optimization of BPCN simulated using a periodic structure.

**Fig. 1.** (a) FT-IR and (b)  $^{13}\text{C}$  CP/MAS ssNMR spectra of PCN (black) and BPCN (blue).

**Fig. 2.** TEM (a, b) and elemental mapping (c, d) images of BPCN (scale bar: 100 nm).

**Fig. 3.** (a) UV-vis DRS and (b) band structures of PCN and BPCN. Integrated PL emission intensity as a function of temperature from 80 to 300 K (Inset: temperature-dependent PL spectra) of (c) PCN and (d) BPCN.

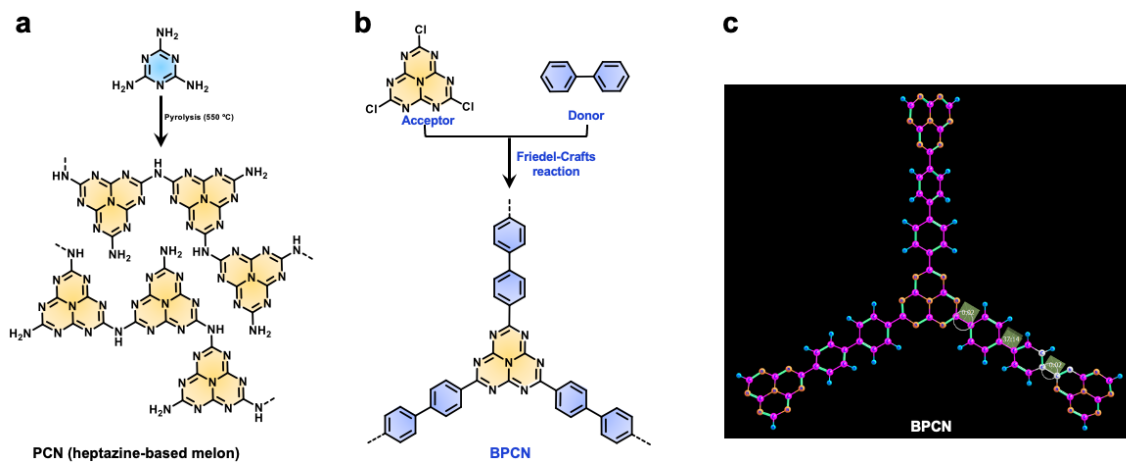
**Fig. 4.** (a) Photocatalytic selective oxidation of thioanisole to methyl phenyl sulfoxide by PCN and BPCN. (b) Recycling experiments of BPCN in the photocatalytic oxidation of thioanisole to sulfoxide.

**Fig. 5.** Proposed reaction mechanisms of thioanisole photo-oxidation by BPCN.

**Fig. 6.** Photocatalytic tests with PCN and BPCN. (a) The  $\text{O}_2$  evolution rates and (b) Time course of the  $\text{O}_2$  production and (c)  $\text{H}_2$  evolution for PCN and BPCN. OER conditions: polymer (50 mg),  $\text{AgNO}_3$  (0.17 g),  $\text{H}_2\text{O}$  (100 mL),  $\lambda \geq 420$  nm, 12 °C; HER conditions: polymer (50 mg), 3% Pt, TEOA/ $\text{H}_2\text{O}$  (10 mL/90 mL),  $\lambda \geq 420$  nm, 12 °C.

**Table 1.** The selective oxidation of sulfides with air over BPCN under blue light ( $\lambda = 450$  nm) irradiation.

**Table 2.** Photocatalytic conversion of various organic molecules using BPCN.



**Scheme 1.**



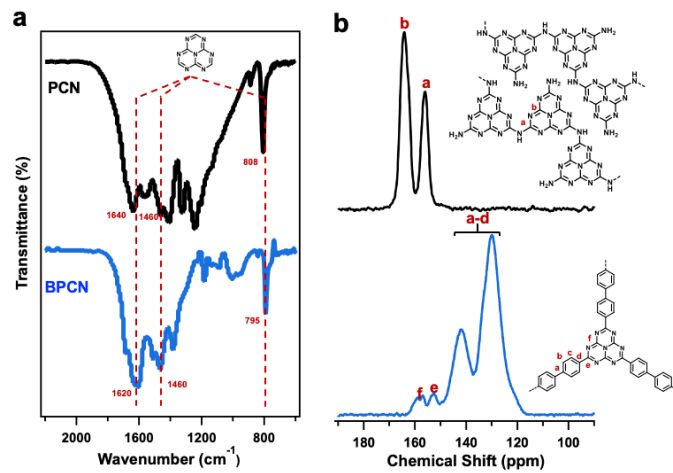
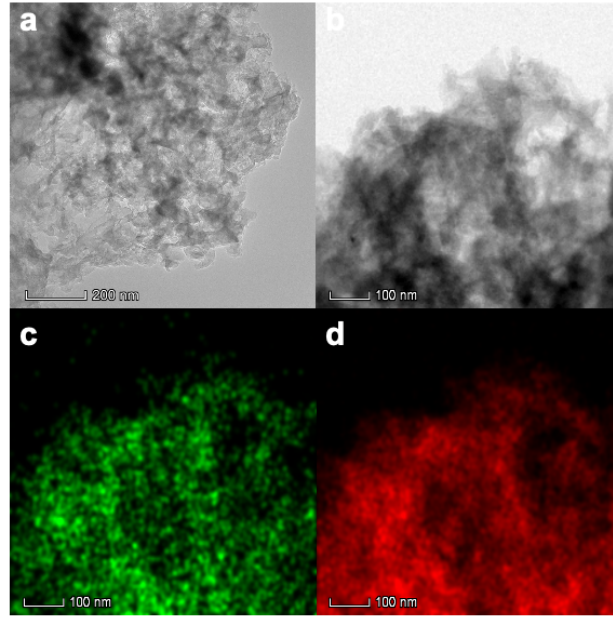


Fig. 1.



**Fig. 2.**

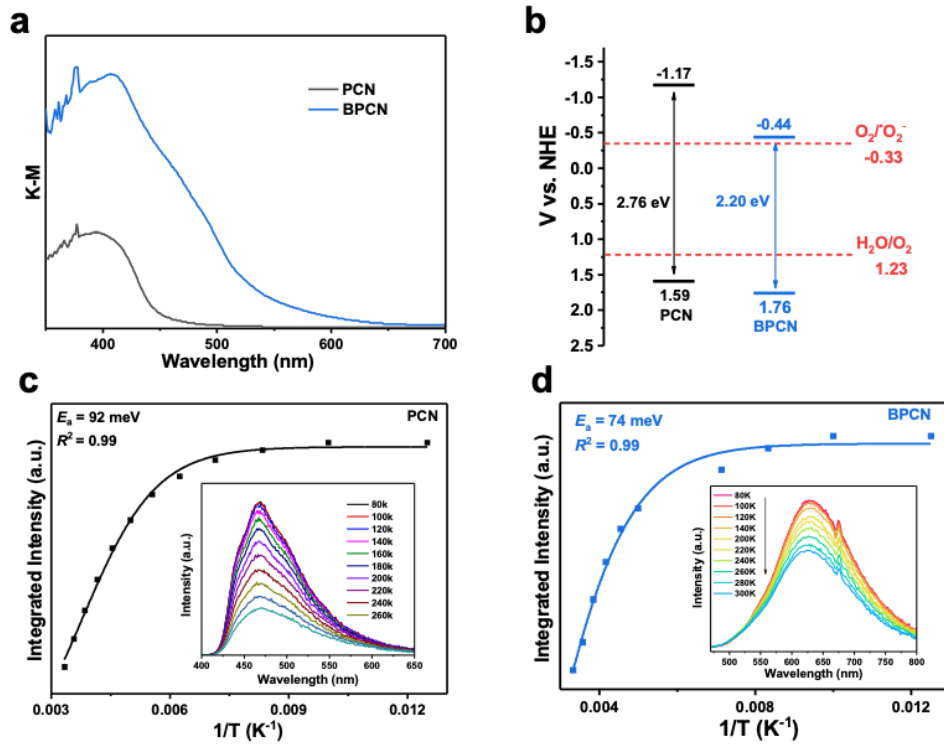
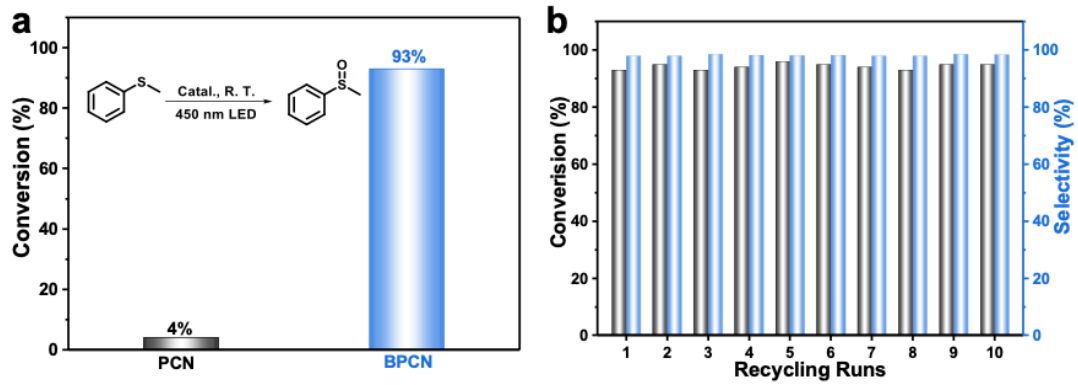


Fig. 3.



**Fig. 4.**

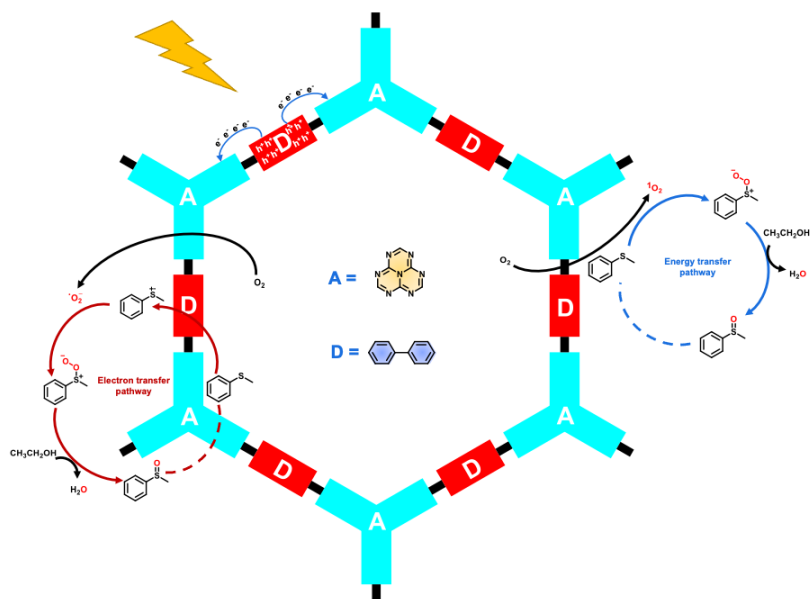


Fig. 5.

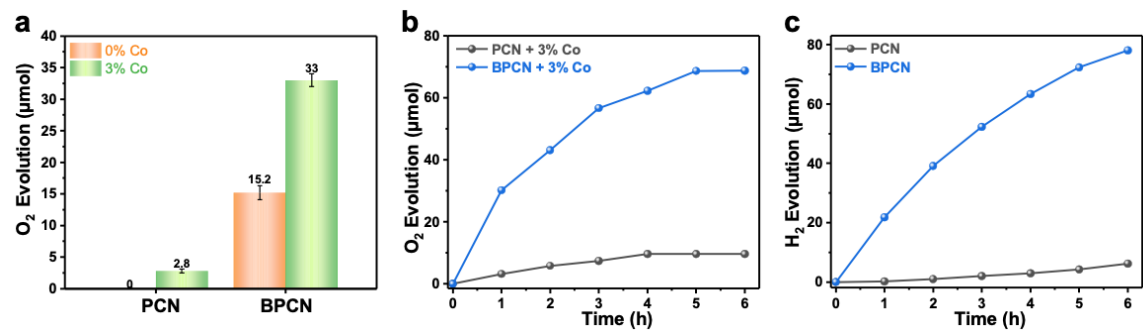
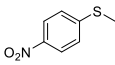
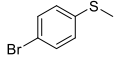
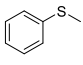
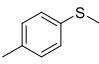
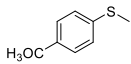
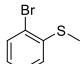
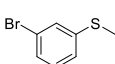
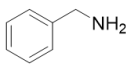
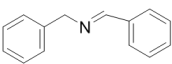
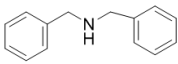
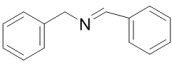


Fig. 6.

**Table 1.**

Entry	Substance	Conv. (%)	Sel. (%)
1		Trace	>99%
2		53	>99%
3		93	>99%
4		96	>99%
5		91	>99%
6		17	>99%
7		32	>99%

**Table 2.**

Entry	Substance	Product	Yield	Sel.
1			98%	>99%
2			99%	>99%
3	Ph-B(OH) <sub>2</sub>	Ph-OH	99%	>99%

<sup>1</sup>Reaction conditions: 0.1 mmol benzylamine, 10 mg Cat., 1 mL acetonitrile, 25 °C, air, 1 h,  $\lambda = 420$  nm.

<sup>2</sup>Reaction condition: 0.1 mmol dibenzylamine, 3 mg Cat., 1 mL acetonitrile, 25 °C, O<sub>2</sub>, 1 h,  $\lambda = 450$  nm.

<sup>3</sup>Reaction condition: 0.5 mmol phenylboronic acid, 10 mg Cat., 3 mL acetonitrile, 1.5 mmol triethylamine, 25 °C, O<sub>2</sub>, 4 h,  $\lambda = 450$  nm.